



1 **Particulate biogenic barium tracer of mesopelagic carbon remineralization in the**
2 **Mediterranean Sea (PEACETIME project)**

3

4 Stéphanie H.M. Jacquet^{1*}, Christian Tamburini¹, Marc Garel¹, Aurélie Dufour¹, France Van-
5 Vambeke¹, Frédéric A.C. Le Moigne¹, Nagib Bhairy¹, Sophie Guasco¹

6

7 ¹Aix Marseille Université, CNRS/INSU, Université de Toulon, IRD, Mediterranean Institute
8 of Oceanography (MIO), UM 110, 13288 Marseille, France

9

10 *Correspondence to: S. Jacquet (stephanie.jacquet@mio.osupytheas.fr)

11

12

13 **Peacetime special issue**

14

15



16 **ABSTRACT**

17 We report on the sub-basins variability of particulate organic carbon (POC)
18 remineralization in the central and western Mediterranean Sea during a late spring period
19 (PEACETIME cruise). POC remineralization rates (MR) were estimated using the excess
20 non-lithogenic particulate barium (Ba_{xs}) inventories in mesopelagic waters (100-1000 m) and
21 compared with prokaryotic heterotrophic production (PHP). MR range from 25 ± 2 to $306 \pm$
22 $70 \text{ mg C m}^{-2} \text{ d}^{-1}$. Results reveal larger MR processes in the Algerian (ALG) basin compared to
23 the Tyrrhenian (TYR) and Ionian (ION) basins. Ba_{xs} inventories and PHP also indicates that
24 significant remineralization occurs over the whole mesopelagic layers in the ALG basin in
25 contrast to the ION and TYR basins where remineralization is mainly located in the upper 500
26 m horizon. We propose that this may be due to particle injection pumps likely driven by
27 strong winter convection in the Western basin of the Mediterranean Sea. This implies
28 significant differences in the remineralization length scale of POC in the central
29 Mediterranean Sea relative to the western region.

30



31 **1. Introduction**

32 In the ocean, remineralization rate associated with sinking particles is a crucial
33 variable for air sea CO₂ balance (Kwon et al., 2009). Most of the sinking particulate organic
34 carbon (POC) conversion (i.e. remineralization) into CO₂ by heterotrophic organisms (i.e.
35 respiration) occurs within the mesopelagic zone (100-1000 m) (Martin et al., 1987; Buesseler
36 et al., 2007; Buesseler and Boyd, 2009). A quantitative representation of this process is thus
37 crucial to future predictions of the ocean's role in the global C cycle (IPCC, 2014). Particulate
38 biogenic barium (Ba_{xs}) is a geochemical tracer of POC remineralization in the mesopelagic
39 layer. Ba_{xs} occurs in the form of barite (BaSO₄ crystals) in the dark ocean as a byproduct of
40 prokaryotic remineralization. In a global ocean undersaturated with respect to barite (Monnin
41 and Cividini, 2006), Ba_{xs} precipitates inside oversaturated biogenic micro-environments
42 during POC degradation by heterotrophic prokaryotes, through sulfate and/or barium
43 enrichment (Dehairs et al., 1980; Stroobant et al., 1991; Bertram and Cowen, 1997;
44 Ganeshram et al., 2003). By applying a transfer function relating Ba_{xs} to O₂ consumption
45 (Dehairs et al., 1997) Ba_{xs} has been widely used since the 90's as an estimator of mesopelagic
46 POC remineralization rates in various sectors of the Southern Ocean, North Pacific and North
47 Atlantic (Cardinal et al., 2001, 2005; Dehairs et al., 2008; Jacquet et al., 2008a, 2008b, 2011,
48 2015; Planchon et al., 2013; Lemaitre et al., 2018). Jacquet et al. (in review) recently reported
49 that such transfer function could be applied in the Mediterranean Sea without restriction. This
50 last study complemented previous investigations aiming at improving the use of Ba_{xs} to
51 estimate local processes of POC remineralization in the Mediterranean Sea (Jacquet et al.,
52 2016; Jullion et al., 2017). In this prospect, the Mediterranean Sea represents a unique case
53 study, mainly due to unresolved issues related to the imbalance in the regional C budget
54 (Sternberg et al., 2008; Santinelli et al., 2010; Tanhua et al., 2013b; Malanotte-Rissoli et al.,
55 2014).



56 The present work is part of the PEACETIME project (ProcEss studies at the Air-sEa
57 Interface after dust deposition in the MEditerranean sea) (<http://peacetime-project.org/>).
58 PEACETIME aimed at studying the chain of processes occurring in the Mediterranean Sea
59 after atmospheric deposition (Saharan dust), and to put them in perspective on-going
60 environmental changes (Guieu et al., in review, this special issue). Dust deposition is a major
61 source of micro- and macro-nutrients that can stimulate the biological carbon pump through
62 organic matter production (i.e. primary production) and its subsequent export and
63 remineralization in the water column (Pabortsava et al., 2017). Overall, the aims of the
64 present contribution to the PEACTIME project were: (1) to document particulate biogenic
65 Ba_{xs} in different ecoregions of the western and central parts of the Mediterranean Sea.
66 Previous Ba_{xs} data in the Mediterranean Sea are relatively scarce with limited vertical
67 sampling resolution (Sanchez-Vidal et al., 2005) or restricted locations (Dehairs et al., 1987;
68 Sternberg et al., 2008); (2) to estimate Ba_{xs} -based POC remineralization rates at mesopelagic
69 depths (MR) according to the Dehairs' transfer function (Dehairs et al., 1997; Jacquet et al., in
70 review), and (3) to determine the relationship between Ba_{xs} and environmental variability,
71 including dust deposition, and (4) assess potential differences in remineralization length scale
72 of POC in the various ecoregions of the Mediterranean Sea.

73

74 **2. Material and methods**

75 **2.1 Study area**

76 The PEACETIME cruise (<https://doi.org/10.17600/17000300>) was conducted during late
77 spring conditions from May 10 to June 11, 2017 (French R/V Pourquoi pas?) in the western
78 and central Mediterranean (Figure 1a). Three main ecoregions (Reygondeau et al., 2014;
79 Ayata et al., 2018) were crossed during the cruise: the Algero-Provençal basin (later referred
80 to as ALG), the Tyrrhenian basin (TYR) and the Ionian basin (ION). The hydrography



81 displays the general three-layer Mediterranean system with surface, intermediate and deep
82 waters (Tamburini et al., 2013; Tanhua et al., 2013b; Hainbucher et al., 2014, Malanotte-
83 Rizzoli et al., 2014). Briefly, the main water masses can be distinguished (see potential
84 temperature – salinity diagram during the PEACETIME cruise in Figure 1b): (1) from west to
85 east surface Atlantic Water (SW) is gradually replaced by Ionian surface Water (ISW) and
86 Levantine Surface water (LSW); (2) Winter Intermediate Water (WIW) and Levantine
87 Intermediate water (LIW). LIW is present at intermediate depths (from 200 to 800 m) and is
88 characterized by a local maximum of salinity and a local minimum of dissolved oxygen
89 concentration; (4) Mediterranean Deep Water (MDW).

90 **2.2 Barium sampling and sample processing**

91 Thirteen stations were sampled for particulate barium from surface to 2000 m (thirty depths
92 in total) in the ALG (stations #1, #2, #3, #10, #Fast, #9 and #4), TYR (stations #5, Tyrr and
93 #6) and ION (stations #8, #7 and #Ion) basins. Three of these stations were sampled twice on
94 different days (long stations #Fast, #Tyrr and #Ion), but due to technical problem no
95 particulate barium data are available for the second visit at station #Ion.

96 We followed the same Ba sample processing and analysis as in Jacquet et al. (2015).
97 Briefly, 4 to 6 L of seawater sampled using Niskin bottles were filtered onto 47 mm
98 polycarbonate membranes (0.4 μm porosity). Filters were rinsed with MQ water grade, dried
99 (50°C) and stored for later analysis. In the laboratory, we performed a total digestion of
100 filters. Solutions were analysed for Ba and other elements of interest (i.e. Al, Sr and Ca) by
101 HR-ICP-MS (High Resolution-Inductively Coupled Plasma- Mass Spectrometry; ELEMENT
102 XR, Thermo).

103 Particulate biogenic barium in excess (hereafter referred to as Ba_{xs}) was calculated as the
104 difference between total Ba and lithogenic Ba using Al as the lithogenic reference element
105 (Dymond et al., 1992; Taylor and Mc.Lennan, 1985). The standard uncertainty (Ellison et al.,



106 2000) on Ba_{xs} concentration ranges between 5.0 and 5.5%. The term “in excess” is used to
107 indicate that concentrations are larger than the Ba_{xs} background. The background (or residual
108 value) is considered as “performed” Ba_{xs} at zero oxygen consumption left over after transfer
109 and partial dissolution of Ba_{xs} produced during degradation of previous particles export
110 events. This background Ba_{xs} value likely depends on the saturation state of the water with
111 respect to barite ($BaSO_4$, the main phase of particulate biogenic barium). Saturation indexes
112 were reported in Jacquet et al. (2016) over a high resolution and quasi-zonal Mediterranean
113 transect (M84/3 cruise; Tanhua et al., 2013a). They revealed that the water column throughout
114 the study area is largely undersaturated, with saturation state ranging between 0.2 and 0.6. A
115 background Ba_{xs} value of 130 pM was recently reported in Jacquet et al. (in review). It is
116 close to the average Ba_{xs} contents observed at greater depth (>1000 m) in the present study
117 (see below).

118 **2.3 Prokaryotic heterotrophic production**

119 Prokaryotic heterotrophic production (PHP) estimation was measured by incorporating L-
120 [4,5- 3H]-Leucine (3H -Leu, 109 [TC1] Ci mmol⁻¹ of specific activity, PerkinElmer®) to get
121 a final saturation concentration of 20 nM in surface until 800 m depth and 10
122 nM [TC2] below 800m depthn, and incubated between 4 hours for sample from 0-200 m
123 depth, 6 hours for sample between 200-800 m depth and 10 hours for sample below 800m
124 depth. Deep prokaryotic heterotrophic production (PHP) was measured over time course
125 experiments at *in situ* temperature in the dark following the protocol described in Tamburini
126 et al. (2002). At the end of incubation, triplicate 40 mL formaldehyde-killed blanks and
127 triplicate 40 mL were incubated at at *in situ* temperature (13°C). At the end of incubation,
128 samples were fixed with 2% final concentration formaldehyde and stored at 4°C until
129 filtration. The detailed protocol is also detailed in Kirchman (1993). Epipelagic layers (0- 250
130 m) were incubated using the microcentrifuge technique at 20 nM final concentrations (see Van



131 Wambeke et al., this issue, submitted). To calculate prokaryotic heterotrophic production, we
132 used the empirical conversion factor of 1.5 ng C per pmol of incorporated leucine according
133 to Simon and Azam (1989). Indeed, isotope dilution was negligible under these saturating
134 concentrations as checked occasionally with concentration kinetics.

135 **2.4 POC remineralization rates**

136 We recently reported on the validity of the Dehairs's transfer function (Dehairs et al., 1997)
137 in the Mediterranean basin to estimate mesopelagic POC remineralization (Jacquet et al., in
138 review). We applied the similar approach to estimate remineralization rates (MR):

$$139 \quad MR = [(Ba_{xs} - Ba_{BKG})/17450] \times Z \times RR \text{ (Eq.1)}$$

140 With Z the depth layer considered and RR the Redfield C/O₂ molar ratio (127/175;
141 Broecker et al., 1985). As reported above, a Ba background (BKG) value of 130 pM was used.

142 **3. Results**

143 Particulate biogenic Ba_{xs}, biogenic Ba fraction (%) and particulate Al, Sr and Ca
144 concentrations are reported in Figure 2 in the upper 2000 m along a zonal transect crossing
145 the three main sub-basins. PHP rates are also reported in Figure 2 in the upper 500 m along
146 the same transect.

147 At stations #9, #Tyrr, #8 and #Ion, Ba_{xs} concentrations in the upper 100 m are quite
148 high (>5000 pM), with values reaching up to 11700 pM (80 m at station #Tyrr) (Figure 2a).
149 The very high Ba_{xs} contents in the surface are quite unusual, though similar values were
150 occasionally observed in earlier Southern Ocean studies (Dehairs et al., 1991, 1997; Jacquet et
151 al., 2007b, 2008a,b). The high Ba_{xs} values at stations #Tyrr and #Ion are associated with
152 higher Sr and Ca concentrations (Figure 2d, e).

153 The upper mesopelagic layer (100-500 m) shows the characteristic large Ba excess
154 (maximum), as illustrated in Figure 3a. The lithogenic impact on the Ba_{xs} signal is relatively
155 low except at stations #4, #5 and #Tyrr where it reached >20 % at some depths in the water



156 column (Figure 2b). The Ba_{xs} maximum at stations in the ALG basin and at station #7 in the
157 ION basin presents a deeper extent compared to stations in the TYR basin (Figure 2a). At
158 station #Ion Ba_{xs} maximum coincides with higher Ca concentrations between 300 and 400 m
159 (Figure 2e). However, the Ba_{xs} maximum is not restricted to the upper mesopelagic layer and
160 also extends deeper. This is especially salient at stations in the ALG basin. At the other
161 stations Ba_{xs} concentrations below 500 m decrease to reach the background value of 130 pM.
162 Among stations sampled twice for barium during the cruise, station #Fast presents similar
163 Ba_{xs} profiles except between 400 and 1000 m with lower concentrations measured during the
164 second visit (3 days later; Figure 3a). In contrast, at station #Tyrr differences between Ba_{xs}
165 profiles mainly occurred in the surface layer and upper mesopelagic layer, with relatively
166 higher Ba_{xs} peaks during the second visit (2 days later).

167 PHP rates decrease from west to east in surface waters (Figure 2f). At station #Fast,
168 PHP rates decreased from 49.4 ng C l⁻¹ h⁻¹ in surface to values between 7.5 and 11.1 ng C l⁻¹
169 h⁻¹ at 100 m depth and below 6.05 ng C l⁻¹ h⁻¹ below 200 m depth (Figure 3d). Same trend can
170 be found in #Tyrr and #Ion stations with a rate in surface waters of around 36 and below 27
171 ng C l⁻¹ h⁻¹ respectively (Figure 3e and 3f).

172 Depth-weighted average (DWA_v) concentrations of Ba_{xs} are reported in Table 1 for
173 the upper (100-500 m) and entire (100-1000 m) mesopelagic layer. Since the base of the
174 mixed layer was generally shallower than 100 m, this depth is taken as the upper boundary of
175 the mesopelagic domain. DWA_v range from 221 to 979 pM. On average stations located in
176 the ALG basin present higher DWA_v than in the TYR and ION basins. DWA_v Ba_{xs} values
177 remained rather stable over the 3-day period at station #Fast and even displayed a slight
178 decrease from 527 to 381 pM (100-1000 m), corroborating above-mentioned profiles
179 variation. In contrast, at station #Tyrr DWA_v Ba_{xs} values for the 100-500 m layer increased
180 from 329 to 810 pM over the 2-day period. Also, for all stations DWA_v Ba_{xs} values globally



181 increase when considering the whole mesopelagic layer, reflecting that significant Ba_{xs} is still
182 extending up to 1000 m depth.

183 **4. Discussion**

184 **4.1 Ba_{xs} distributions across the sub-basins**

185 The very high Ba_{xs} concentrations reported in the surface layer at stations #9, #Tyrr,
186 #8 and #Ion are associated with Sr and Ca maxima, likely linked with potentially ballasted
187 phytoplankton-derived material. Similar observations were previously reported in the
188 Southern Ocean, revealing that in the surface water particulate Ba_{xs} is incorporated into or
189 adsorbed onto biogenic material, with barite being a minor component (Dehairs et al., 1991,
190 1997; Jacquet et al., 2007a, 2008a, b). Below the surface layer, Ba_{xs} presents the characteristic
191 maximum reflecting remineralization processes in the mesopelagic layer. The maximum
192 extends up to 1000 m in the ALG and ION basins, while it is mostly located in the upper 500
193 m in the TYR basin. The lithogenic impact on the Ba_{xs} signal is relatively low, except at
194 stations #4, #5 and #Tyrr where it is moderated. A dust deposition event occurred over a large
195 area including the southern Tyrrhenian Sea during PEACETIME, starting on May 10 (Guieu
196 et al., this issue) at the beginning of the campaign. Particulate Al concentrations and estimated
197 lithogenic Ba fraction were sampled at these stations 5 to 12 days after the event and would
198 potentially reflect a slight impact of this dust event in depth.

199

200 **4.2 Mesopelagic Ba_{xs} and prokaryotic heterotrophic production**

201 Previous studies highlighted the relationship between the mesopelagic Ba_{xs} and the
202 vertical distribution of prokaryotic heterotrophic production (PHP), reflecting the temporal
203 progression of POC remineralization processes. Figure 3d-f shows PHP profiles in the upper
204 2000 m at long station #Fast, #Tyrr and #Ion. The whole dataset is discussed in Van
205 Wambeke et al. (submitted, this issue). Figure 4 shows column-integrated PHP at 100 m over



206 column-integrated PHP at 500 m vs. DWAv Ba_{xs} calculated over the entire 100-500 m depth
207 interval. Results are confronted to the relationships obtained in the Southern Ocean (Jacquet
208 et al., 2008a, 20015) and recently in the northeast Atlantic and northwestern Mediterranean
209 Sea (PAP and ANTARES/EMSO-LO observatory sites, respectively) (Jacquet et al., in
210 review). Results during PEACETIME follow the same trend, indicating higher DWAv Ba_{xs} in
211 situation where a significant part of column-integrated PHP is located deeper in the water
212 column (high $Int.PHPx1/IntPHPx2$ ratio, Figure 4). During KEOPS2, the lowest DWAv were
213 reported for stations located in a meander and reflected the occurrence of different (earlier)
214 stages of bloom advancement compared to the other stations (see “season advancement” in
215 Figure 4). Similarly, station #5 and #Tyrr2 would reflect the temporal evolution of the
216 establishment of mesopelagic remineralization processes in the TYR basin compared to the
217 other basins. Measurements performed during the second visit at station #Tyrr4 two days later
218 corroborate this hypothesis and would potentially reflect an increase of remineralization
219 processes in the upper mesopelagic depths.

220 **4.3 Mesopelagic C remineralization**

221 We translated mesopelagic Ba_{xs} DWAv into POC remineralization rates (MR) using Equ.
222 (1). Figure 5 reports MR rates for the upper and entire mesopelagic layer. MR range from 25
223 ± 2 to 306 ± 70 $mg\ C\ m^{-2}\ d^{-1}$. We observe a large difference in MR rates in the ALG basin
224 depending on the integration depths. This is especially salient at station #9. These results
225 reveal significant remineralization occurred between 500 and 1000 m. In contrast, in the ION
226 and TYR basins MR rates reflect that remineralization is mainly located in the upper 500 m
227 horizon. As mentioned above, stations in the TYR region experienced a dust event and our
228 particulate Al concentrations and estimated lithogenic Ba fraction presented a slight impact of
229 this event. Despite the small increase in MR rates at station #Tyrr between the two visits, we
230 can wonder whether the overall impact of the dust event could result in lower and upper



231 mesopelagic layer-restricted MR processes. This would suggest that by providing ballast
232 material (dust), and thereby decreasing of the exposition time of particles to prokaryotic
233 remineralization (Pabortsava et al., 2017), the dust event reduced MR at station #Tyrr.
234 Another dust event occurred on June 5 a few hours after the first sampling at station #Fast in
235 the ALG basin. Again, it is very interesting to observe a decrease in MR rates between the
236 two visits in the 500-1000 m depth layer at station #Fast. However, station #Fast does not
237 present any evidence of an impact on particulate Al concentrations and estimated lithogenic
238 Ba fraction. Furthermore, it is obvious that, in contrast to variables change in the surface
239 layer, observable response in mesopelagic Ba_{xs} and remineralization processes to a single dust
240 event would require continuous observations over few days to week, from an initial state just
241 before the event to a complete process of POC production, subsequent export and
242 remineralization.

243 Overall, the present study indicates that the ALG basin is the place where higher
244 mesopelagic remineralization processes occur. These new results confirm previous work of
245 Jullion et al. (2017) reporting dissolved Ba and Parametric Optimum Multiparameter (POMP)
246 calculation-derived POC remineralization fluxes (from 156 to 348 mg C m⁻² d⁻¹). These
247 authors showed significant differences in the mesopelagic MR between the west and the east
248 of the Mediterranean basin, suggesting an additional export pathway and subsequent
249 remineralization driven by the winter deep convection in the western basin. By providing a
250 detailed Ba_{xs} dataset in the ALG, TYR and ION sub-basin, the present work would confirm
251 the hypothesis of particle injection pump (Boyd et al., 2019) at western stations in the
252 Mediterranean Sea.

253

254 **5. Conclusion**

255 The present paper presents an expended dataset on the Ba_{xs} distribution in the western and



256 central Mediterranean Sea in late spring 2017. Our results reveal the Ba_{xs} distribution globally
257 extends deeper in the ALG basin. Derived MR fluxes are also higher in this basin. The
258 relationship between DW_{Av} Ba_{xs} and PHP in the mesopelagic layer corroborates the trend of
259 higher Ba_{xs} in situation of significant deeper PHP activity and subsequent remineralization.

260

261 **Acknowledgments**

262 This study is a contribution to the PEACETIME project (<http://peacetime-project.org>), a
263 joint initiative of the MERMEX and ChArMEx components supported by CNRS-INSU,
264 IFREMER, CEA, and Météo-France as part of the programme MISTRALS coordinated by
265 INSU. PEACETIME was endorsed as a process study by GEOTRACES. We thank the
266 captain and the crew of the RV Pourquoi Pas? for their professionalism and their work at sea.
267 We warmly thank C. Guieu and K. Deboeufs, as coordinators of the program PEACETIME.
268 Part of the equipment used in this work was funded in 2012 by European Regional
269 Development Fund (ERDF). The project leading to this publication has received funding from
270 European FEDER Fund under project 1166-39417.



271 **Figures**

272

273 Figure 1: (a) Map of the study area showing the three sub-basins (ALG, TYRR and ION) with
274 stations' locations; (b) Potential temperature – salinity diagram with isopycnals (kg m^{-3}) for
275 PEACETIME profiles. Graph constructed using Ocean Data View (Schlitzer, 2002).

276

277 Figure 2: (a-e) Sections of particulate biogenic Ba (Ba_{xs} , pM), Al (pM), Sr (pM) and Ca (nM)
278 concentrations, and % Ba_{xs} (biogenic fraction) in the upper 2000 m water column. (f) Section
279 of PHP ($\text{ngC L}^{-1} \text{h}^{-1}$) is reported in the upper 500 m. Graph constructed using Ocean Data
280 View (Schlitzer, 2002).

281

282 Figure 3: Ba_{xs} (a-c; pM) and PHP (d-f; $\text{ngC L}^{-1} \text{h}^{-1}$) profiles in the upper 2000 m at long
283 stations #Fast, #Tyrr and #Ion.

284

285 Figure 4: Integrated PHP in the upper 100 m over integrated PHP in the upper 500 m versus
286 depth-weighted average (DWA) mesopelagic Ba_{xs} (pM) over the 150-500 depth interval
287 during PEACETIME. The same relations are reported for KEOPS1 and KEOPS2 cruises
288 (Southern Ocean; Jacquet et al., 2015) and at the PAP (NE-Atlantic) and ANTARES/EMSO-
289 LO (NW-Mediterranean Sea) observatory sites (Jacquet et al., in review, biogeosciences).

290

291 Figure 5: POC remineralization fluxes ($\text{mg C m}^{-2} \text{d}^{-1}$) in the upper (100-500 m) and entire
292 (100-1000 m) mesopelagic layer in the ALG, TYR and ION basins.

293

294



295 **Tables**

296 Table 1: Depth-weighted average (DWA_v) concentrations of Ba_{xs} (pM) and remineralization
297 rates (MR; mg C m⁻² d⁻¹) for the upper (100-500 m) and entire (100-1000 m) mesopelagic
298 layer.



299 **References**

- 300 Ayata, Sakina-Dorothee, Jean-Olivier Irisson, Anaïs Aubert, Léo Berline, Jean-Claude Dutay,
301 Nicolas Mayot, Anne-Elise Nieblas, et al. “Regionalisation of the Mediterranean Basin, a
302 MERMEX Synthesis.” *Progress in Oceanography* 163 (2018): 7–20.
303 doi:https://doi.org/10.1016/j.pocean.2017.09.016.
- 304 Bertram, Miriam, and James P. Cowen. “Morphological and Compositional Evidence for
305 Biotic Precipitation of Marine Barite.” *Journal of Marine Research* 55 (1997): 577–93.
- 306 Boyd, Philip, Hervé Claustre, Marina Levy, David Siegel, and Thomas Weber. “Multi-
307 Faceted Particle Pumps Drive Carbon Sequestration in the Ocean.” *Nature* 568 (April 1,
308 2019): 327–35. doi:10.1038/s41586-019-1098-2.
- 309 Broecker, Wallace S. “‘NO’, a Conservative Water-Mass Tracer.” *Earth and Planetary
310 Science Letters* 23, no. 1 (August 1974): 100–107. doi:10.1016/0012-821X(74)90036-3.
- 311 Buesseler, Ken O., Carl H. Lamborg, Philip W. Boyd, Phoebe J. Lam, Thomas W. Trull,
312 Robert R. Bidigare, James K. B. Bishop, et al. “Revisiting Carbon Flux Through the
313 Ocean’s Twilight Zone.” *Science* 316, no. 5824 (2007): 567–70.
314 doi:10.1126/science.1137959.
- 315 Buesseler, Ken O., and Philip W. Boyd. “Shedding Light on Processes That Control Particle
316 Export and Flux Attenuation in the Twilight Zone of the Open Ocean.” *Limnology and
317 Oceanography* 54, no. 4 (2009): 1210–32. doi:10.4319/lo.2009.54.4.1210.
- 318 Cardinal, Damien, Frank Dehairs, Thierry Cattaldo, and Luc André. “Geochemistry of
319 Suspended Particles in the Subantarctic and Polar Frontal Zones South of Australia:



- 320 Constraints on Export and Advection Processes.” *Journal of Geophysical Research:*
321 *Oceans* 106, no. C12 (décembre 2001): 31637–56. doi:10.1029/2000JC000251.
- 322 Cardinal, Damien, Nicolas Savoye, Thomas W. Trull, Luc André, Elzbieta E. Kopczynska,
323 and Frank Dehairs. “Variations of Carbon Remineralisation in the Southern Ocean
324 Illustrated by the Baxs Proxy.” *Deep Sea Research Part I: Oceanographic Research*
325 *Papers* 52, no. 2 (février 2005): 355–70. doi:10.1016/j.dsr.2004.10.002.
- 326 Dehairs, F., R. Chesselet, and J. Jedwab. “Discrete Suspended Particles of Barite and the
327 Barium Cycle in the Open Ocean.” *Earth and Planetary Science Letters* 49, no. 2
328 (September 1980): 528–50. doi:10.1016/0012-821X(80)90094-1.
- 329 Dehairs, F., S. Jacquet, N. Savoye, B. A. S. Van Mooy, K. O. Buesseler, J. K. B. Bishop, C.
330 H. Lamborg, et al. “Barium in Twilight Zone Suspended Matter as a Potential Proxy for
331 Particulate Organic Carbon Remineralization: Results for the North Pacific.” *Deep Sea*
332 *Research Part II: Topical Studies in Oceanography*, Understanding the Ocean’s
333 Biological Pump: results from VERTIGO, 55, no. 14–15 (juillet 2008): 1673–83.
334 doi:10.1016/j.dsr2.2008.04.020.
- 335 Dehairs, F., C. E. Lambert, R. Chesselet, and N. Risler. “The Biological Production of Marine
336 Suspended Barite and the Barium Cycle in the Western Mediterranean Sea.”
337 *Biogeochemistry* 4, no. 2 (June 1, 1987): 119–40. doi:10.1007/BF02180151.
- 338 Dehairs, F., D. Shopova, S. Ober, C. Veth, and L. Goeyens. “Particulate Barium Stocks and
339 Oxygen Consumption in the Southern Ocean Mesopelagic Water Column during Spring
340 and Early Summer: Relationship with Export Production.” *Deep Sea Research Part II:*
341 *Topical Studies in Oceanography* 44, no. 1–2 (1997): 497–516. doi:10.1016/S0967-
342 0645(96)00072-0.



- 343 Dehairs, F., N. Stroobants, and L. Goeyens. “Suspended Barite as a Tracer of Biological
344 Activity in the Southern Ocean.” *Marine Chemistry* 35, no. 1–4 (1991): 399–410.
345 doi:[http://dx.doi.org/10.1016/S0304-4203\(09\)90032-9](http://dx.doi.org/10.1016/S0304-4203(09)90032-9).
- 346 Dymond, J.R., Suess, E., Lyle, M.: Barium in deep-sea sediment: a geochemical proxy for
347 paleoproductivity, *Paleoceanography*, 7, 163–181, 1992.
- 348 Ellison, Eurachem/CITAC Guide CG4, Quantifying Uncertainty in Analytical Measurement.
349 Eds. S.L.R. Ellison, M. Rosslein and A. Williams. Second edition ISBN 0948926 15 5,
350 Pp 120, 2000.
- 351 Ganeshram, Raja S., Roger François, Judy Commeau, and Susan L. Brown-Leger. “An
352 Experimental Investigation of Barite Formation in Seawater.” *Geochimica et*
353 *Cosmochimica Acta* 67, no. 14 (July 15, 2003): 2599–2605. doi:10.1016/S0016-
354 7037(03)00164-9.
- 355 Guieu et al., this issue. Process studies at the air-sea interface after atmospheric deposition in
356 the Mediterranean Sea: objectives and strategy of the PEACETIME oceanographic
357 campaign (May-June 2017).
- 358 Hainbucher, D., A. Rubino, V. Cardin, T. Tanhua, K. Schroeder, and M. Bensi.
359 “Hydrographic Situation during Cruise M84/3 and P414 (spring 2011) in the
360 Mediterranean Sea.” *Ocean Sci.* 10, no. 4 (juillet 2014): 669–82. doi:10.5194/os-10-669-
361 2014.
- 362 IPCC Working Group 1, 5th Assessment Report (AR5) Climate Change 2013, Published in Jan. 2014.
- 363 Jacquet, S. H. M., F. Dehairs, I. Dumont, S. Becquevort, A. -J. Cavagna, and D. Cardinal.
364 “Twilight Zone Organic Carbon Remineralization in the Polar Front Zone and



- 365 Subantarctic Zone South of Tasmania.” *Deep Sea Research Part II: Topical Studies in*
366 *Oceanography*, Biogeochemistry of the Australian Sector of the Southern Ocean, 58, no.
367 21–22 (November 2011): 2222–34. doi:10.1016/j.dsr2.2011.05.029.
- 368 Jacquet, S. H. M., F. Dehairs, M. Elskens, N. Savoye, and D. Cardinal. “Barium Cycling
369 along WOCE SR3 Line in the Southern Ocean.” *Marine Chemistry* 106, no. 1–2 (juillet
370 2007b): 33–45. doi:10.1016/j.marchem.2006.06.007.
- 371 Jacquet, S. H. M., F. Dehairs, D. Lefèvre, A. J. Cavagna, F. Planchon, U. Christaki, L. Monin,
372 L. André, I. Closset, and D. Cardinal. “Early Spring Mesopelagic Carbon
373 Remineralization and Transfer Efficiency in the Naturally Iron-Fertilized Kerguelen
374 Area.” *Biogeosciences* 12, no. 6 (March 17, 2015): 1713–31. doi:10.5194/bg-12-1713-
375 2015.
- 376 Jacquet, S. H. M., F. Dehairs, N. Savoye, I. Obernosterer, U. Christaki, C. Monnin, and D.
377 Cardinal. “Mesopelagic Organic Carbon Remineralization in the Kerguelen Plateau
378 Region Tracked by Biogenic Particulate Ba.” *Deep Sea Research Part II: Topical*
379 *Studies in Oceanography*, KEOPS: Kerguelen Ocean and Plateau compared Study, 55,
380 no. 5–7 (March 2008a): 868–79. doi:10.1016/j.dsr2.2007.12.038.
- 381 Jacquet, S. H. M., J. Henjes, F. Dehairs, A. Worobiec, N. Savoye, and D. Cardinal.
382 “Particulate Ba-Barite and Acantharians in the Southern Ocean during the European Iron
383 Fertilization Experiment (EIFEX).” *Journal of Geophysical Research* 112, no. G4
384 (October 23, 2007a). doi:10.1029/2006JG000394.
- 385 Jacquet S.H.M., Lefèvre D., Tamburini C., Garel M., Le Moigne F., Bhairy N., Roumagnac
386 M., Guasco S. (in review, *Biogeosciences*). On the barium – oxygen consumption



387 relationship in the Mediterranean Sea: implications for mesopelagic marine snow
388 remineralization.

389 Jacquet, S. H. M., N. Savoye, F. Dehairs, V. H. Strass, and D. Cardinal. “Mesopelagic Carbon
390 Remineralization during the European Iron Fertilization Experiment.” *Global
391 Biogeochemical Cycles* 22, no. 1 (March 1, 2008b): GB1023.
392 doi:10.1029/2006GB002902.

393 Jacquet, S.H.M., C. Monnin, V. Riou, L. Jullion, and T. Tanhua. “A High Resolution and
394 Quasi-Zonal Transect of Dissolved Ba in the Mediterranean Sea.” *Marine Chemistry* 178
395 (January 20, 2016): 1–7. doi:10.1016/j.marchem.2015.12.001.

396 Jullion, L., S. H. M. Jacquet, and T. Tanhua. “Untangling Biogeochemical Processes from the
397 Impact of Ocean Circulation: First Insight on the Mediterranean Dissolved Barium
398 Dynamics.” *Global Biogeochemical Cycles* 31, no. 8 (2017): 1256–70.
399 doi:10.1002/2016GB005489.

400 Kirchman DL (1993) Leucine incorporation as a measure of biomass production by
401 heterotrophic bacteria. In: Kemp PF, Sherr BF, Sherr EB, Cole JJ (eds) Handbooks of
402 methods in aquatic microbial ecology. Lewis Publishers, Boca Raton, Ann Arbor,
403 London, Tokyo, p 509–512

404 Kwon, E. Y., Primeau, F., and Sarmiento, J. L. (2009). The impact of remineralization depth
405 on the air--sea carbon balance. *Nat. Geosci.* 2. doi:10.1038/NGEO612.

406 Lemaitre, N., H. Planquette, F. Planchon, G. Sarthou, S. Jacquet, M. I. García-Ibáñez, A.
407 Gourain, et al. “Particulate Barium Tracing of Significant Mesopelagic Carbon



- 408 Remineralisation in the North Atlantic.” *Biogeosciences* 15, no. 8 (2018): 2289–2307.
409 doi:10.5194/bg-15-2289-2018.
- 410 Malanotte-Rizzoli, P., V. Artale, G. L. Borzelli-Eusebi, S. Brenner, A. Crise, M. Gacic, N.
411 Kress, et al. “Physical Forcing and Physical/biochemical Variability of the
412 Mediterranean Sea: A Review of Unresolved Issues and Directions for Future Research.”
413 *Ocean Science* 10, no. 3 (2014): 281–322. doi:10.5194/os-10-281-2014.
- 414 Monnin, Christophe, and Damien Cividini. “The Saturation State of the World’s Ocean with
415 Respect to (Ba,Sr)SO₄ Solid Solutions.” *Geochimica et Cosmochimica Acta* 70, no. 13
416 (juillet 2006): 3290–98. doi:10.1016/j.gca.2006.04.002.
- 417 Martin, John H., George A. Knauer, David M. Karl, and William W. Broenkow. “VERTEX:
418 Carbon Cycling in the Northeast Pacific.” *Deep Sea Research Part A. Oceanographic*
419 *Research Papers* 34, no. 2 (1987): 267–85. doi:http://dx.doi.org/10.1016/0198-
420 0149(87)90086-0.
- 421 Pabortsava, Katsiaryna, Richard S. Lampitt, Jeff Benson, Christian Crowe, Robert
422 McLachlan, Frédéric A. C. Le Moigne, C. Mark Moore, et al. “Carbon Sequestration in
423 the Deep Atlantic Enhanced by Saharan Dust.” *Nature Geoscience* 10, no. 3 (March 1,
424 2017): 189–94. doi:10.1038/ngeo2899.
- 425 Planchon, F., A.-J. Cavagna, D. Cardinal, L. André, and F. Dehairs. “Late Summer Particulate
426 Organic Carbon Export and Twilight Zone Remineralisation in the Atlantic Sector of the
427 Southern Ocean.” *Biogeosciences* 10, no. 2 (2013): 803–20. doi:10.5194/bg-10-803-
428 2013.



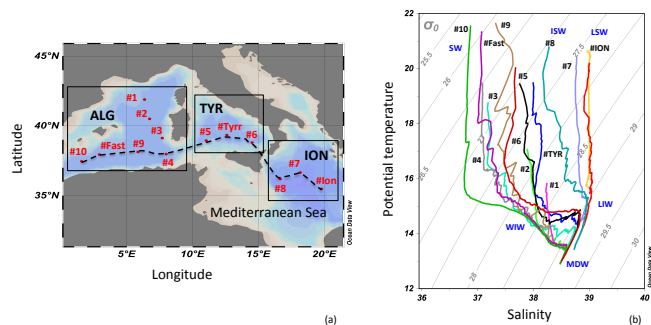
- 429 Reygondeau, Gabriel, Cécile Guieu, Fabio Benedetti, Jean-Olivier Irisson, Sakina-Dorothee
430 Ayata, Stéphane Gasparini, and Philippe Koubbi. “Biogeochemical Regions of the
431 Mediterranean Sea: An Objective Multidimensional and Multivariate Environmental
432 Approach.” *Progress in Oceanography* 151 (2017): 138–48.
433 doi:<http://dx.doi.org/10.1016/j.pocean.2016.11.001>.
- 434 Sanchez-Vidal, A., R. W. Collier, A. Calafat, J. Fabres, and M. Canals (2005), Particulate
435 barium fluxes on the continental margin: A study from the Alboran Sea (Western
436 Mediterranean), *Mar. Chem.*, 93, 105–117.
- 437 Santinelli, Chiara, Luciano Nannicini, and Alfredo Seritti. “DOC Dynamics in the Meso and
438 Bathypelagic Layers of the Mediterranean Sea.” *Deep Sea Research Part II: Topical
439 Studies in Oceanography*, Ecological and Biogeochemical Interactions in the Dark
440 Ocean, 57, no. 16 (août 2010): 1446–59. doi:[10.1016/j.dsr2.2010.02.014](https://doi.org/10.1016/j.dsr2.2010.02.014).
- 441 Schlitzer, R., Ocean Data View, <http://www.awi-bremerhaven.de/GEO/ODV>, 2003.
- 442 Simon M, Azam F (1989) Protein content and protein synthesis rates of planktonic marine
443 bacteria. *Mar Ecol Prog Ser* 51:201–213
- 444 Sternberg, E., C. Jeandel, E. Robin, and M. Souhaut. “Seasonal Cycle of Suspended Barite in
445 the Mediterranean Sea.” *Geochimica et Cosmochimica Acta* 72, no. 16 (2008): 4020–34.
446 doi:<https://doi.org/10.1016/j.gca.2008.05.043>.
- 447 Stroobants, N., F. Dehairs, L. Goeyens, N. Vanderheijden, and R. Van Grieken. “Barite
448 Formation in the Southern Ocean Water Column.” *Marine Chemistry*, Biochemistry and
449 circulation of water masses in the Southern Ocean International Symposium, 35, no. 1–4
450 (November 1991): 411–21. doi:[10.1016/S0304-4203\(09\)90033-0](https://doi.org/10.1016/S0304-4203(09)90033-0).



- 451 Tamburini C, Canals M, Durieu de Madron X, Houpert L, Lefèvre D, Martini S, D’Ortenzio
452 F, Robert A, Testor P, and the ANTARES collaboration (2013) Deep-sea
453 bioluminescence blooms after dense water formation at the ocean surface. PLoS One
454 8:e67523
- 455 Tamburini C, Garcin J, Ragot M, Bianchi A (2002) Biopolymer hydrolysis and bacterial
456 production under ambient hydrostatic pressure through a 2000 m water column in the
457 NW Mediterranean. Deep Res II 49:2109–2123
- 458 Tanhua, T., D. Hainbucher, V. Cardin, M. Álvarez, G. Civitarese, A. P. McNichol, and R. M.
459 Key. “Repeat Hydrography in the Mediterranean Sea, Data from the
460 <i>Meteor&/i> Cruise 84/3 in 2011.” *Earth System Science Data* 5, no. 2
461 (July 31, 2013b): 289–94. doi:10.5194/essd-5-289-2013.
- 462 Tanhua, T., D. Hainbucher, K. Schroeder, V. Cardin, M. Álvarez, and G. Civitarese. “The
463 Mediterranean Sea System: A Review and an Introduction to the Special Issue.” *Ocean
464 Sci.* 9, no. 5 (September 6, 2013a): 789–803. doi:10.5194/os-9-789-2013.
- 465 Taylor, S.R., McLennan, S.M.: The continental crust: its composition and evolution,
466 Blackwell Scientific Publications, 312pp, 1985.
- 467 Van Wambeke, F., Pulido, E., Dinasquet, J., Djaoudi, K., Engel, A., Garel, M., Gusaco, S.,
468 Nunige, S., Taillandier, V., Zäncker, B., and Tamburini, C.: Spatial patterns of biphasic
469 ectoenzymatic kinetics related to biogeochemical properties in the Mediterranean Sea,
470 Biogeosciences Discuss. , bg-2020-253, submitted, 2020
- 471
472
473



474 Figure 1

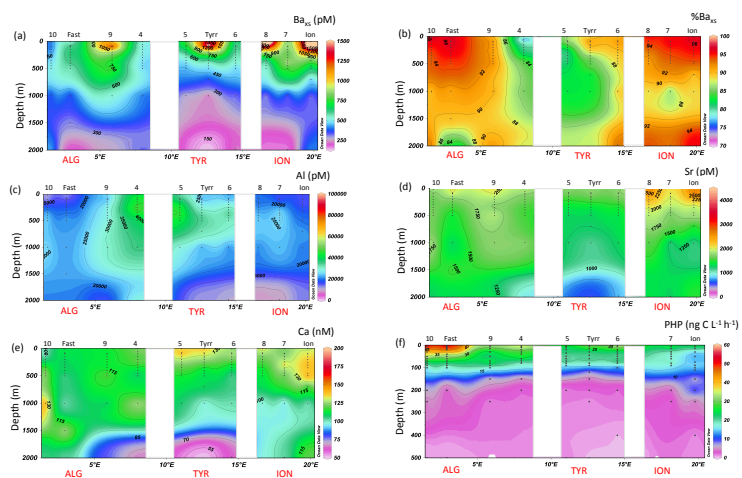


475

476



477 Figure 2

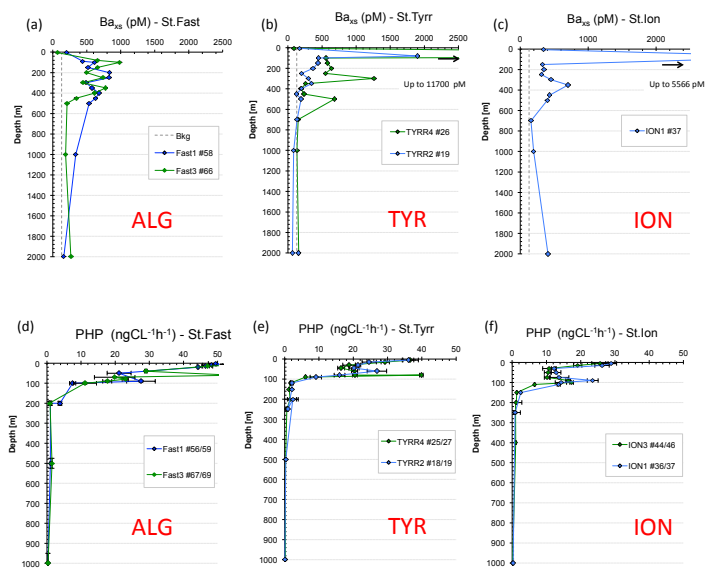


478

479



480 Figure 3

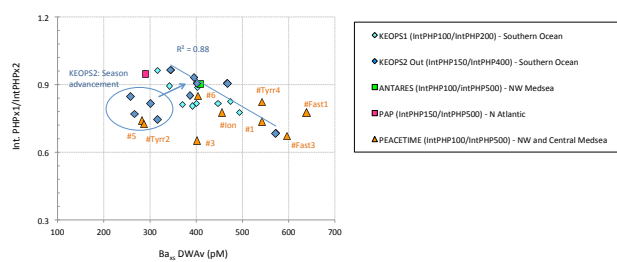


481

482



483 Figure 4

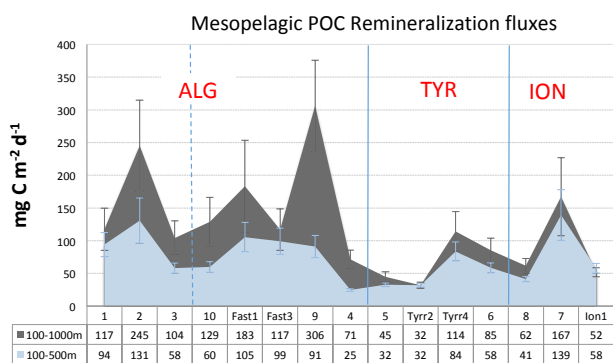


484

485



486 Figure 5



487

488



489 Table 1

Basin	Station #	Mesopelagic layer	DWAv Ba _{xs} [pM]	MR [mg C m ⁻² d ⁻¹]	Std error (%)
Algero-Provençal	1	upper	542	94	20
	1	entire	374	117	27
	2	upper	717	131	26
	2	entire	645	245	28
	3	upper	402	58	13
	3	entire	353	104	25
	4	upper	243	25	8
	4	entire	281	71	20
	9	upper	981	91	19
	9	entire	979	306	23
	Fast1	upper	638	105	21
	Fast1	entire	527	183	38
	Fast3	upper	596	99	20
	Fast3	entire	381	117	27
	10	upper	418	60	13
	10	entire	410	129	29
Tyrrhenian	5	upper	283	32	9
	5	entire	226	45	17
	Tyrr2	upper	284	32	9
	Tyrr2	entire	200	32	15
	Tyrr4	upper	542	84	17
	Tyrr4	entire	380	114	26
	6	upper	404	58	13
	6	entire	313	85	22
Ionian	7	upper	769	139	28
	7	entire	485	167	36
	ION	upper	456	58	13
	ION	entire	315	52	13
	8	upper	363	41	10
	8	entire	273	62	18

490

491